Hindawi Publishing Corporation
International Journal of Photoenergy
Volume 2012, Article ID 849062, 9 pages
doi:10.1155/2012/849062

Research Article

Mesoporous TiO_2 Micro-Nanometer Composite Structure: Synthesis, Optoelectric Properties, and Photocatalytic Selectivity

Kun Liu,[1] Lianjie Zhu,[1] Tengfei Jiang,[2] Youguang Sun,[1] Hongbin Li,[1] and Dejun Wang[2]

[1] *School of Chemistry & Chemical Engineering, Tianjin University of Technology, Tianjin 300384, China*
[2] *College of Chemistry, Jilin University, Changchun 130023, China*

Correspondence should be addressed to Lianjie Zhu, zhulj@tjut.edu.cn

Received 21 April 2012; Accepted 23 April 2012

Academic Editor: Jiaguo Yu

Mesoporous anatase TiO_2 micro-nanometer composite structure was synthesized by solvothermal method at 180°C, followed by calcination at 400°C for 2 h. The as-prepared TiO_2 was characterized by X-ray diffraction (XRD), scanning electron microscope (SEM), transmission electron microscope (TEM), and Fourier transform infrared spectrum (FT-IR). The specific surface area and pore size distribution were obtained from N_2 adsorption-desorption isotherm, and the optoelectric property of the mesoporous TiO_2 was studied by UV-Vis absorption spectrum and surface photovoltage spectra (SPS). The photocatalytic activity was evaluated by photodegradation of sole rhodamine B (RhB) and sole phenol aqueous solutions under simulated sunlight irradiation and compared with that of Degussa P-25 (P25) under the same conditions. The photodegradation preference of this mesoporous TiO_2 was also investigated for an RhB-phenol mixed solution. The results show that the TiO_2 composite structure consists of microspheres (~0.5–2 μm in diameter) and irregular aggregates (several hundred nanometers) with rough surfaces and the average primary particle size is 10.2 nm. The photodegradation activities of this mesoporous TiO_2 on both RhB and phenol solutions are higher than those of P25. Moreover, this as-prepared TiO_2 exhibits photodegradation preference on RhB in the RhB-phenol mixture solution.

1. Introduction

In recent decades, TiO_2 has received considerable attention due to its wide applications in fields such as solar cell, photocatalysis and lithium-ion batteries [1–9]. As a potential excellent catalyst, TiO_2 has a great prospect in waste water treatment [10–12]. However, in order to commercialize this technique, a few problems need to be solved at the first time: (1) preparation of catalyst with high specific surface area; (2) extending the light absorption capability of the catalyst to visible region; (3) easy separation of the catalyst from the suspension after photodegradation. It was known that monodispersed nanocrystalline TiO_2 generally has high specific surface area and high photocatalytic activity. But normally it suffers from severe aggregation during photocatalytic reactions, which would reduce its active sites and light harvesting capability. As a result, its photocatalytic activity would be decreased. Moreover, it is too small to be separated from the suspension by conventional method. Hence, in recent years, mesoporous TiO_2 microspheres have received much attention because the porous structures would offer a high specific surface area, and the large particle size causes them to be separated and reclaimed easily since they can settle down in aqueous suspensions by gravity [13]. However, increasing the particle size of a catalyst is often accompanied by a decrease in its photocatalytic activity, while a large-sized mesoporous micro-nanometer TiO_2 composite structure with high specific surface area may solve this problem. A facile route for large-scale synthesis of such TiO_2 photocatalyst may benefit practical applications of this photocatalysis technique in industrial waste water treatment.

Among the synthesis methods, hydrothermal or solvothermal method was often applied extensively [13–15] because of its simple, mild, and uniform crystallization. In the present paper, mesoporous micro-nanometer TiO_2 composite structures were synthesized by solvothermal

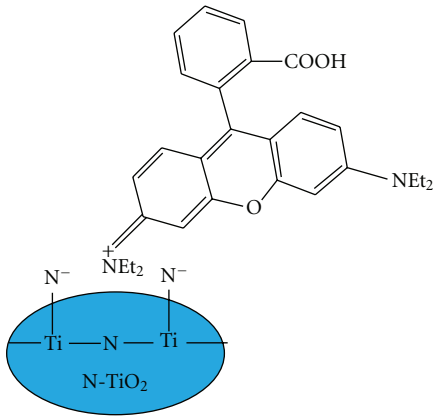

Scheme 1: Adsorption mode of RhB on the surface of N-doping TiO_2.

method. Since dye sensitization can easily extend the light absorption capability of the TiO_2 catalyst to visible region [16, 17], RhB was used to evaluate the photocatalytic activity of the as-prepared TiO_2 under simulated sunlight irradiation because the RhB itself can act as a sensitizer. Furthermore, photodegradation of phenol aqueous solution over this TiO_2 composite structure was also investigated because phenol is one of the common organic pollutants that can hardly adsorb the visible light.

Since it is usual that several organic pollutants are present simultaneously in the real effluents from industries and photocatalytic oxidation process based on TiO_2 was found a highly effective method for degradation of organic pollutants, studying the preferential degradation of organic pollutants in their mixture solutions over TiO_2 catalysts is important for the practical application. Some researchers have been devoted to this problem [18–23]. For example, Comparelli et al. [18] have explored the effect of two different substituents on photodegradation of two organic dyes, methyl red and methyl orange. Sahel et al. [20] have studied the photocatalytic degradation of a mixture of two anionic dyes, remazol black and red procion MX-5B. Yu et al. [21–23] have investigated photocatalytic selectivity towards decomposition of azo dyes, methyl orange, methyl blue, or methyl violet. But so far the preferential photodegradation by a mesoporous TiO_2 in an RhB-phenol mixture solution has been hardly seen. Therefore, we choose an RhB-phenol mixed aqueous solution as a model system to investigate the photodegradation preference of the TiO_2 catalyst.

2. Experimental

2.1. Preparation of TiO_2. In a typical procedure, 0.1 mL of triethanolamine was added to 40 mL of absolute ethanol (99%) and kept stirring for a few minutes. Then, 1.5 mL of tetrabutyl titanate was dropped into the solution under vigorous stirring and a white suspension was obtained. After 4 h stirring, the suspension was transferred to a 50 mL Teflon-lined stainless steel autoclave and kept in an electric oven at 180°C for 24 h. The autoclave was taken out and left to cool naturally to the room temperature. A white precipitate was obtained via centrifugation, washed with ethanol for two times, and dried at 60°C for 6 h. Finally, the product was calcined at 400°C for 2 h with a heating rate of 1°C min^{-1} to obtain the mesoporous TiO_2.

2.2. Characterization. X-ray powder diffraction (XRD) measurements were performed on a Rigaku D/max-2500 diffractometer with Cu Kα radiation (λ = 0.154056 nm) at 40 kV and 100 mA. Scanning electron microscope (SEM) images were taken with a JSM 6700F field-emission scanning electron microscope. Transmission electron microscope (TEM) and high-resolution TEM (HRTEM) images were obtained with a JEOL JEM-2100F transmission electron microscope operating at 200 kV. UV-Vis diffuse reflectance absorption spectra were recorded on a Hitachi/U-3900 UV-visible spectrophotometer. N_2 adsorption-desorption isotherm was obtained with a V-Sorb 2800P surface area and pore size analyzer. FT-IR spectrum was carried out on a Nicolet Avatar 370 Fourier transform infrared spectrometer. The XPS measurement was performed on a PHI-5300 ESCA system. Surface photovoltage spectrum (SPS) was measured by a homemade sandwich-type solid junction cell ITO/Sample/ITO with light monochromator-lock-in detection technique, and filed induced surface photovoltage spectra (FISPS) were obtained with aid of a DC electric field applied to two sides of the sample cell. The SPS data have been normalized to make the light intensity of the lamp the same at each wavelength. Details on the setup have been described elsewhere [24]. The absorbance of the RhB or phenol aqueous solutions during the photocatalytic reactions was examined by a UV-2100 UV-visible spectrophotometer. The relative concentration of RhB and phenol in their mixed solution at certain photodegradation time was measured by a COMETRO LC6000 high-performance liquid chromatography (HPLC).

2.3. Photocatalytic Activity Measurement. Photocatalytic activity of the mesoporous TiO_2 was investigated by photodegradations of RhB (10 mg L^{-1}) and phenol (10 mg L^{-1}) aqueous solutions under simulated sunlight illumination, where a 400 W halogen light (from Beijing Lighting Research Institute) was used as the light source to simulate the sunlight (with ~5% UV light). The photocatalysis system and reaction conditions were described in our previous work [25]. The concentration of RhB at certain reaction time was determined by measuring its absorbance at 552 nm on a UV-visible spectrophotometer, from which the photodegradation percentage was calculated by using the formula $\Phi = (A_0 - A)/A_0 \times 100\%$, where Φ is the degradation percentage, A_0 the initial absorbance of the RhB solution, and A the absorbance at certain reaction time. The photodegradation of phenol aqueous solution over the mesoporous TiO_2 was studied by following the same procedure as above, but the absorbance at 270 nm was measured for the phenol solution.

3. Results and Discussion

3.1. Crystal Phase and Morphology of the Mesoporous TiO_2. The high crystallinity and phase purity of the calcined sample

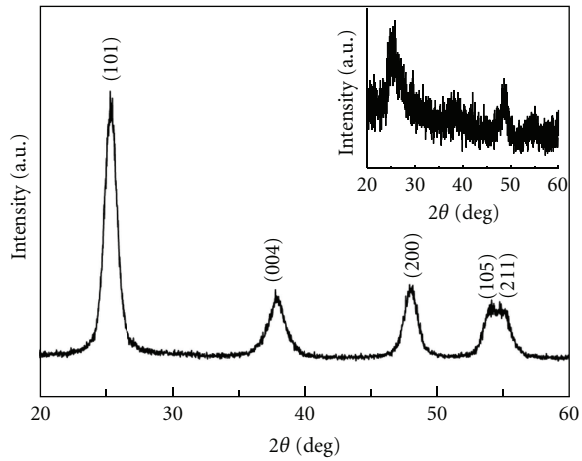

FIGURE 1: XRD patterns of the as-prepared TiO_2 after calcination at 400°C and before calcination (the inset).

TiO_2 were characterized by XRD, as shown in Figure 1. All of the diffraction peaks can be indexed to anatase TiO_2 (JCPDS card no. 04-0477, space group $I4_1/amd$ (141), and cell $a = 3.785$ Å, $c = 9.514$ Å). The average primary particle size of the as-prepared TiO_2 was calculated by using the Debye-Scherrer formula based on the 101 diffraction peak, which is 10.2 nm. The weak and broad peaks in the inset of Figure 1 indicate a bad crystallinity of the uncalcined TiO_2 sample. Therefore, the calcination of the pristine product at 400°C for 2 h with a heating rate of 1°C min^{-1} led to a great increase in its crystallinity, but the anatase crystal phase was kept unchanged.

The morphology and microstructure of the as-obtained TiO_2 are clearly demonstrated by SEM, TEM, and HRTEM images, as shown in Figures 2 and 3. It is apparent (Figures 2(a) and 2(b)) that only part of the products possess microspherical structure with diameters of 0.5–2 μm. The most part is irregular aggregate with sizes of several hundred nanometers. Whatever the shape of the product is,0020 it is constructed by numerous interconnected primary nanocrystals and the surface is rather rough. The TEM images (Figures 3(a) and 3(b)) confirm the porous nature of the product with the main pore size of around 10 nm and the primary nanocrystal size of around 10 nm as well, which is consistent with the XRD result. These nanocrystals are connected with each other and the pores are the interparticle voids. The HRTEM image shows that many anatase primary nanocrystals are random in orientations. The lattice spacings for all the chosen adjacent three nanocrystals are measured to be 0.351 nm, as marked in Figure 3(c), corresponding to the (101) facet of the anatase phase. The fast Fourier transform (FFT) pattern (inset) displays somewhat dispersed spots with circles, which implies it is a multicrystalline.

3.2. N_2 Adsorption-Desorption Isotherm. Figure 4 shows the nitrogen adsorption-desorption isotherm of the as-synthesized TiO_2, which is characteristic of a type IV isotherm with a type H3 hysteresis loop, indicating the presence of mesopores in the size range of 2–50 nm. As depicted in the Barrett-Joyner-Halenda (BJH) pore size distribution (the inset of Figure 4), the main pore sizes are in the range of 2–20 nm and the pore volume is 0.490 $cm^3\ g^{-1}$. The Brunauer-Emmett-Teller-(BET-) specific surface area is as high as 179 $m^2\ g^{-1}$, which may be benefit to its high photocatalytic activity.

3.3. FT-IR Spectrum. Figure 5(a) shows the FT-IR spectrum of the mesoporous TiO_2. The peaks at 464 cm^{-1} and 530 cm^{-1} are characteristic stretching vibrations of Ti–O–Ti network in TiO_2, and the bands around 3420 cm^{-1} and 1650 cm^{-1} could be assigned to the stretching and bending vibrations of the O–H group and adsorbed water, respectively [26]. The bands between 900 and 1300 cm^{-1} could be attributed to the stretching vibration of C–O or C–N bond [27], which might be from the residual of the triethanolamine. This could be further clarified by the following results.

As shown in Figures 5(b)–5(d), the XPS results confirmed that the products contain some residual nitrogen on the surface of TiO_2. The nitrogen percentage in the whole N-doping TiO_2 sample is small, ca. 1.4% (atomic ratio), but the N/Ti atomic ratio is as high as 0.1 : 1, which is far beyond the environmental contamination level (ca. 0.01 : 1 in the P25 sample [28]). This clearly indicates the N-doping in this mesoporous TiO_2. The peak of N 1s around 400.16 eV can be assigned to the N atom in the environment of O–Ti–N [29] or Ti–O–N [30]. The peak around 397 eV is attributable to N mainly interacting with Ti centers [31, 32]. The nitrogen element comes from the only source triethanolamine. According to the XPS result in C 1s region, three peaks were observed (after the Gaussian fitting) with binding energies of 284.8 eV, 286.4 eV, and 288.9 eV. They can be assigned to C–C, C–O, and C=O groups, respectively, by referring to [33], where these three peaks were attributed to adventitious carbon species from XPS measurement. No obvious signal at ~282 eV, corresponding to O–Ti–C bond, was observed in our case, which implies that no carbon doping occurred.

3.4. Optoelectric Properties. The light-harvesting capabilities of the as-prepared mesoporous TiO_2 and the P25 are slightly different, as shown in Figure 6(a). Besides the strong intrinsic absorption below 400 nm, the TiO_2 sample can also weakly absorb the visible light (400–700 nm), which was not observed for the P25. This, on the one hand, indicates a stronger light scattering ability of the as-prepared TiO_2 due to its larger particle sizes [1] of the microspherical and irregular aggregate structures. On the other hand, it could be attributed to the impurity states deriving from nitrogen insertion in the bulk of the oxide or intrinsic defects, including those defects associated with oxygen vacancies [34, 35]. The calculated band gap energy of the mesoporous TiO_2, 3.15 eV, by using the method in [36] is much higher than that of the P25, 2.95 eV, which is attributed to the quantum size effect because the average primary particle size of the sample TiO_2, 10.2 nm, is much smaller than that of P25, ~25 nm.

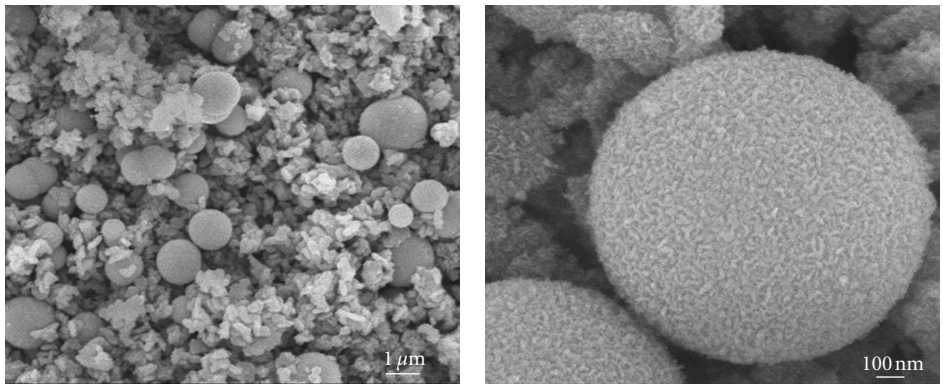

(a) (b)

Figure 2: SEM images of the as-prepared TiO_2: (a) low magnification, (b) high magnification.

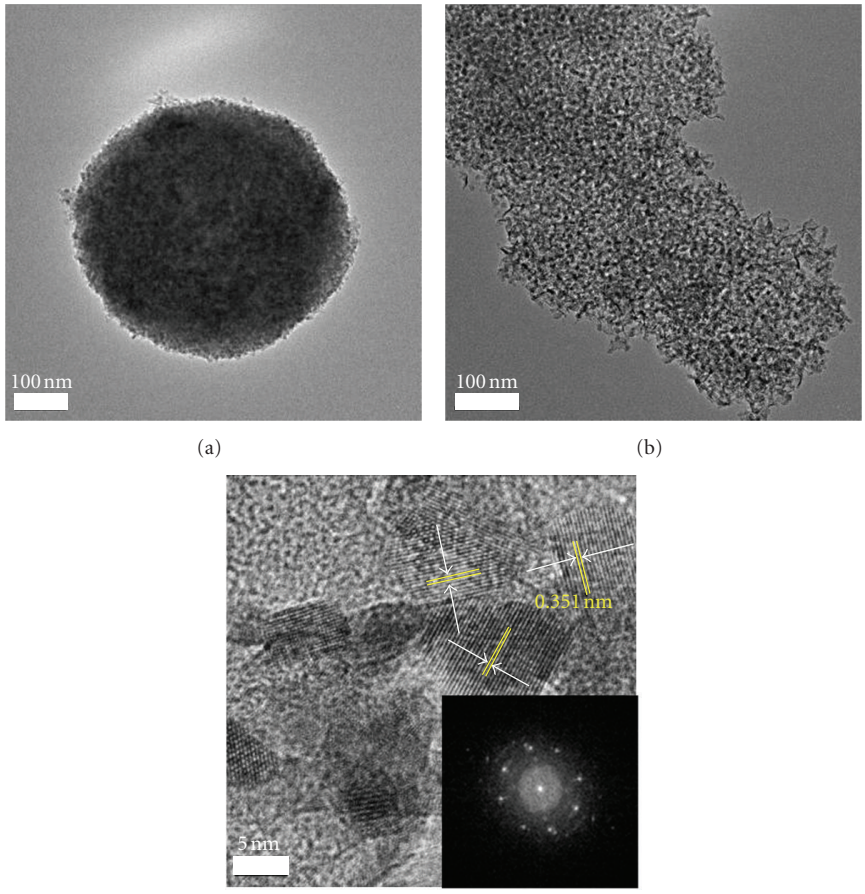

(a) (b)

(c)

Figure 3: ((a) and (b)) TEM images. (c) HRTEM image and fast Fourier transform (FFT) pattern (inset) of the as-prepared mesoporous TiO_2.

Surface photovoltage spectrum (SPS) is a well-established contactless and nondestructive technique for semiconductor characterization, which can reflect the separation and recombination of photo-induced electron-hole pairs on the catalyst surface under illumination [37]. When the incident light energy is higher than the band gap energy of TiO_2, the electrons are excited from the valence band to the conduction band, which generates the electron-hole pairs. The electrons move to the surface and the holes to the bulk of the TiO_2 by the built-in electric field, which generates photovoltage signal. As shown in Figure 6(b), a pronounced surface photovoltage signal is observed in the

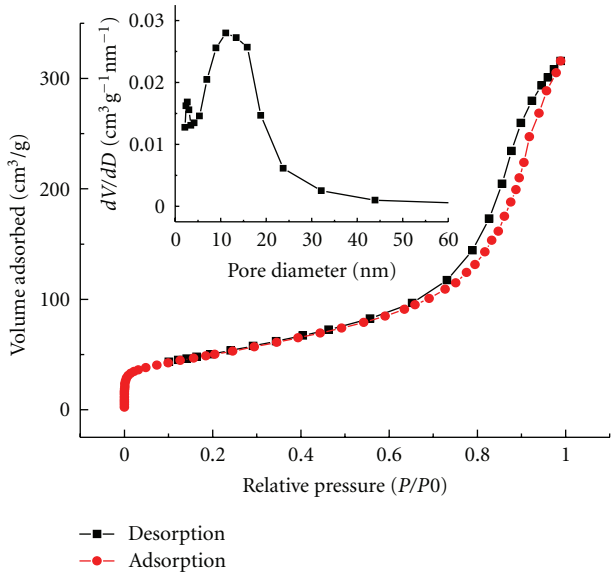

FIGURE 4: N_2 adsorption-desorption isotherm of the as-prepared mesoporous TiO_2, and the inset is the BJH pore-size distribution curve.

range of 300–425 nm, which includes two transition bands according to the Gaussian fitting (the inset of Figure 6(b)). Besides an intrinsic band-band transition from 300 nm to 375 nm ($O_{2p} - Ti_{3d}$ at 335 nm [38]), there is a sub-band-gap transition with the peak value of around 365 nm, which is attributed to the electron transition from valence band to surface state, deriving from the surface impurity. This impurity state in the mesoporous TiO_2 locates at 0.3 eV below the conduction band according to the calculation using the formula $x = 1240/y$. Here, x is the energy level and y is the wavelength at the responding peak. According to the fitting result, as shown in the inset of Figure 6(b), 335.6 nm and 365 nm are used for calculations of energy levels of the conduction band and surface state, respectively. Referring to the method in [39], by making a tangent line across the band edge of the SPS (see Figure 6(b)), the Eg of the mesoporous TiO_2 is calculated again, which is 3.23 eV, higher than the value obtained based on the absorption spectrum. This Eg value is more consistent with its quantum size of 10 nm. Therefore, SPS is a good method for accurately determining band gap energy of a semiconductor because SPS exactly reflects the electron transition behavior under illumination.

When a 0.5 V positive external electric field was applied to the sample, the surface photovoltage signal increases, which indicates that the direction of the external electric field is the same with that of the built-in electric field. On the contrary, it decreases in a 0.5 V negative electric field. These imply that this mesoporous TiO_2 exhibits a p-type semiconductor according to the field effect principle [40]. This p-type semiconductor character may be due to the surface impurity, a little nitrogen, which is consistent with the results of FT-IR, XPS, and UV-Vis absorption spectra.

3.5. Photocatalysis. The photocatalytic activity of the as prepared TiO_2 was first estimated on the basis of the decomposition of RhB under simulated sunlight illumination. Degussa P25 was used as the reference material for comparison purpose. In the controlled experiment in which RhB was in the mesoporous TiO_2 suspensions in dark for 2 h, no obvious photocatalytic activity (<5%) was observed. However, the photolysis rate of RhB was serious, about 45%, in the absence of TiO_2 catalyst. Figures 7(a) and 7(b) present the photodegradation curves of RhB aqueous solutions under simulated sunlight irradiation, which demonstrate that both the sample TiO_2 and P25 exhibit high photocatalytic activities. This may be due to self-sensitization of the RhB dye on the TiO_2 catalyst, which extends the wavelength range for light absorption of the TiO_2 catalyst to the visible light region. Although the photodegradation activities of the sample TiO_2 and P25 on RhB solutions are similar, the sample TiO_2 would benefit from its larger particle sizes because it can be easily reclaimed under gravity from the suspension after reactions. The results show that the suspension of the sample TiO_2 settled down mostly after 5 min and completely after 18 min, whereas for P25 suspension no obvious change was observed after 30 min sedimentation. On the other hand, the larger particle sizes may reduce aggregate of the catalyst to a certain extent. It was well known that aggregation of nanosized TiO_2 was very difficult to avoid, and these aggregates can actually affect the number of the active sites, light scattering property of the TiO_2, and the photon penetration [41]. In the end it will reduce the photocatalytic activity of the catalyst. In general the smaller crystals are poorer light scatterer than the larger crystals as the scattering efficiency is proportional to r^4 in Rayleigh scattering [42]. With the reaction going on, the P25 gradually forms aggregates, which would reduce its active sites and scatter more incident photons because these aggregates are constructed by larger size of primary crystals (~25 nm) than the sample TiO_2 (10.2 nm). The decrease in active sites and light absorption capability would result in a decrease in its photocatalytic activity. As for the TiO_2, there would be no such serious aggregation in the case of its large particle size. Moreover, the high specific surface area offers the as-prepared catalyst a big number of active sites and the porous micro-nanometer composite structure allows a great number of scattered photons to penetrate into the mesopores so that the interior of the microspheres and irregular aggregates could be utilized for photodegradation reactions as well to a certain extent. These may explain the higher photocatalytic activity of the as-prepared TiO_2 at the latter stage of the photodegradation reaction.

No obvious degradations of the phenol aqueous solutions (10 mg L^{-1}) were observed (<5%) over the sample TiO_2 in the dark and photolysis in the absence of TiO_2 catalyst. Under simulated sunlight irradiation, the photodegradation percentage of phenol aqueous solution over the as-prepared TiO_2 is always higher than that of P25, see Figures 7(c) and 7(d). It reaches 49.3% after 2 h reactions, which is higher than that of P25 (38%). This high photocatalytic activity may be related with its high specific surface area. Moreover, the existence of the surface state, as shown in Figure 6(b), can reduce the recombination of the photogenerated electron-holes since the photogenerated electrons can transfer to the

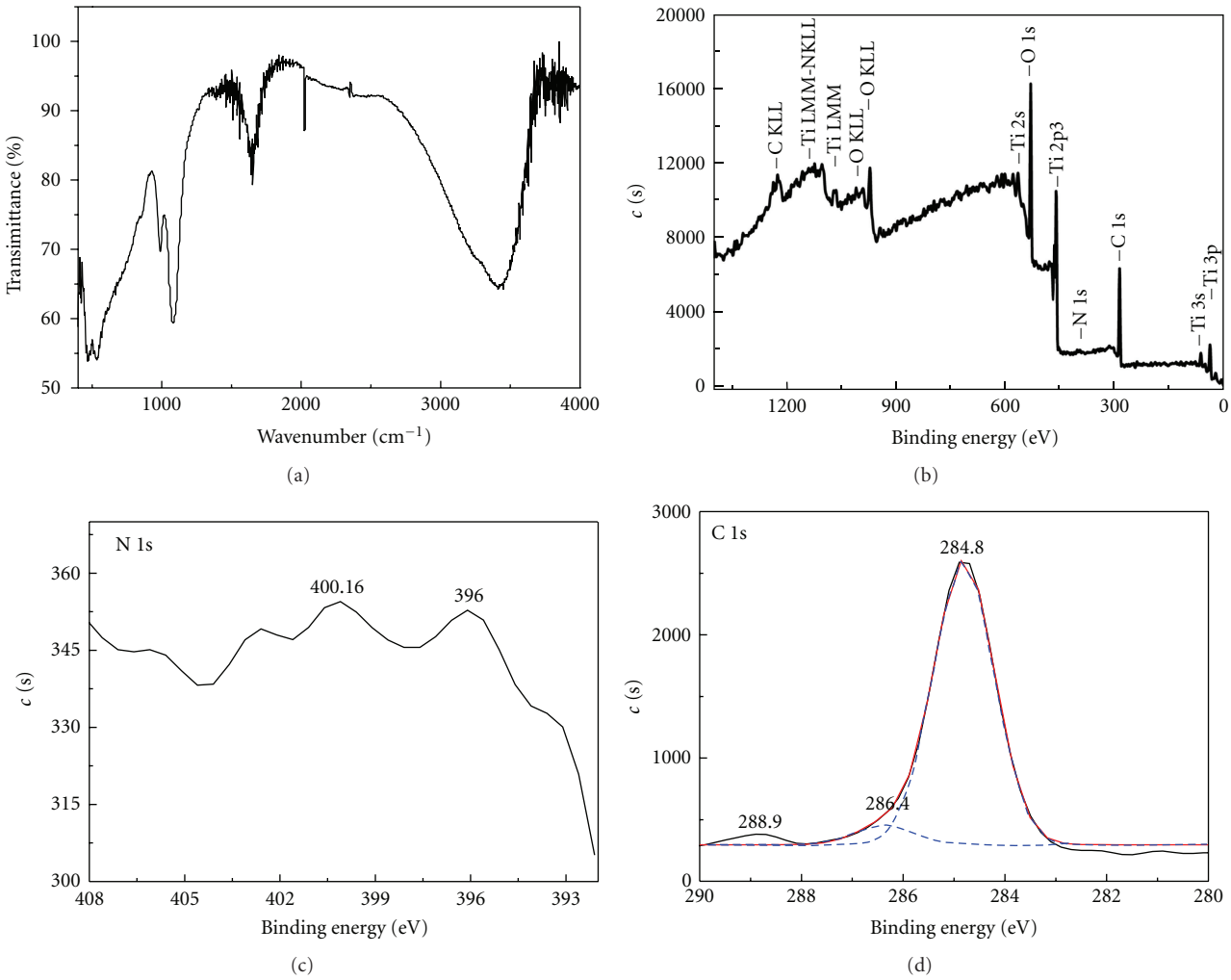

Figure 5: (a) FT-IR of the mesoporous TiO_2. ((b)–(d)) XPS of the mesoporous TiO_2: survey (b) and deconvoluted spectra for N 1s (c) and C 1s (d).

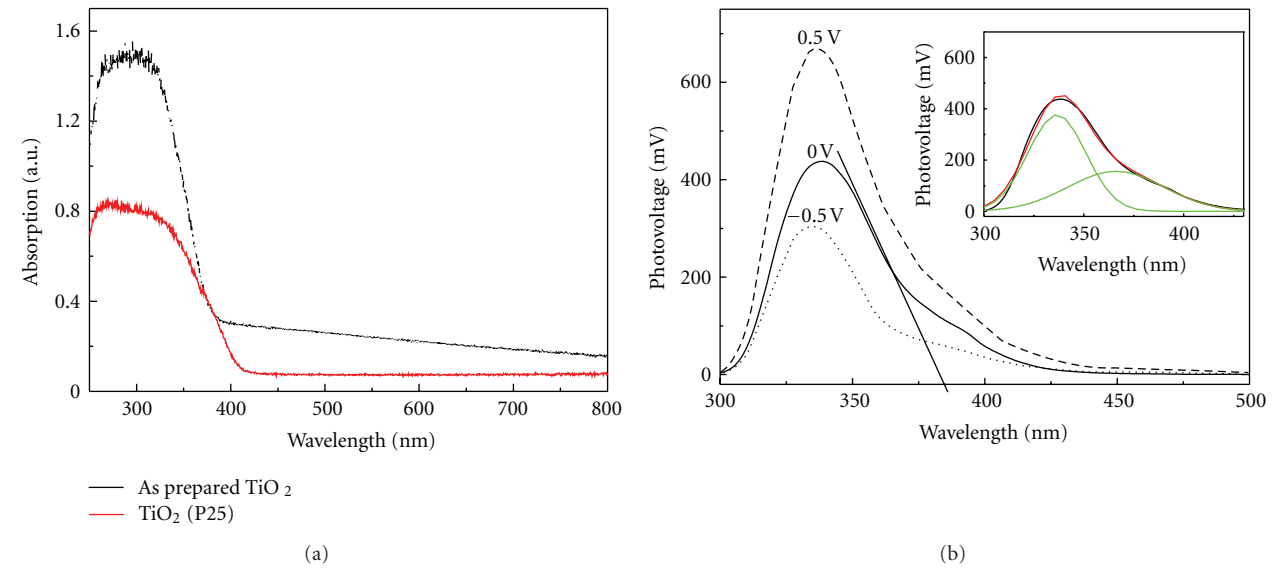

Figure 6: (a) UV-Vis diffuse reflection absorption spectra of the as-prepared mesoporous TiO_2 and P25. (b) Surface photovoltage spectrum (SPS) and field-induced surface photovoltage spectra (FISPS) of the mesoporous TiO_2, and the inset is the Gaussian fitting of the SPS.

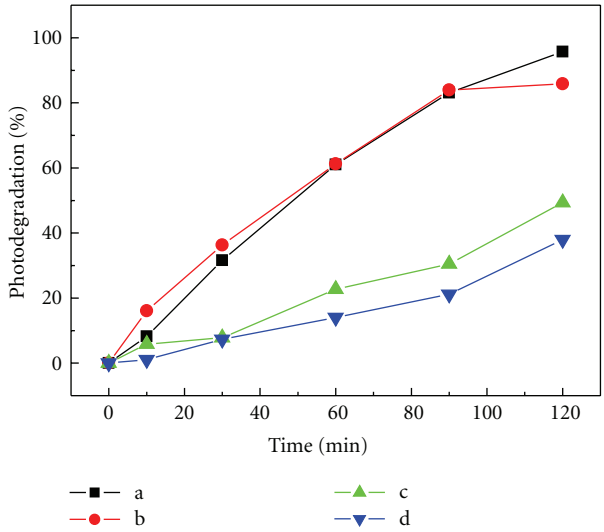

Figure 7: Photocatalytic performance of the as-prepared mesoporous TiO_2 and P25 under simulated sunlight irradiation: photodegradations of (a) the mesoporous TiO_2 on RhB, (b) P25 on RhB, (c) the mesoporous TiO_2 on phenol, and (d) P25 on phenol.

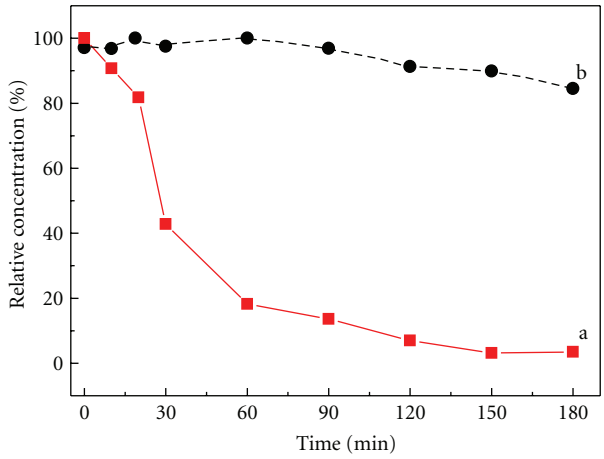

Figure 8: Photodegradation preference of the as-prepared TiO_2 on RhB and phenol in their mixture solution under simulated sunlight: (a) RhB, (b) phenol.

surface state. As a result, the photocatalytic activity will be increased. From the microstructure point of view, the porous structure of the sample TiO_2 also benefits the photon penetration and separation of photogenerated carriers. Thus, the photocatalytic activity will be increased.

Since the presence of organic pollutant mixtures in real effluents from industries is frequent, we studied the preferential photodegradation of a RhB-phenol mixed solution over the as-prepared mesoporous TiO_2 under simulated sunlight irradiation, as shown in Figure 8 where HPLC was used to monitor the relative concentration of the two organics in their mixture solution at any reaction time and the maximum absorption wavelengths (552 nm for RhB and 270 nm for phenol) were chosen, respectively, for the measurement. The concentration of RhB and phenol in the mixture solution is the same, 10 mg L^{-1}. It is obvious that the as-prepared TiO_2 exhibits much higher photocatalytic activity on RhB than phenol. The relative concentration of RhB drops to 18.2% after 1 h photodegradation reaction. At the same time, however, the relative concentration of phenol hardly changes (<5%). In the next reaction stage, from 1 h to 3 h, the residual RhB was decomposed completely and phenol was simultaneously degraded slightly. The photodegradation percentage of phenol in three hours is only 15.5%, which is much lower than that for the sole phenol aqueous solution (49.3%, as shown in Figure 7(c)). These results suggest that the simultaneous presence of RhB in the solution disturbs and postpones the photodegradation of phenol. It also implies that the RhB could not function as a sensitizer for the TiO_2 catalyst to increase the visible light utilization and photodegradation efficiency of phenol in the RhB-phenol mixture solution system.

The photodegradation preference on RhB in the mixed solution may be caused by the preferential adsorption of RhB molecules. It was reported [43–45] that RhB preferentially anchors on an F-doping TiO_2 through the cationic moiety (–NEt_2 group). Similarly, it could also adsorb on the N-doping TiO_2 surface through the NEt_2 group, as shown in Scheme 1. Here, the cationic –NEt_2 group has strong static electron interaction with the anionic N atom on the TiO_2 surface. Moreover, the RhB molecule can absorb UV-visible light in the range of 200–600 nm, whereas the phenol only absorbs the light below 280 nm. This could also be responsible partially for the higher photodegradation activity of RhB in the mixed solution.

4. Conclusions

Mesoporous anatase TiO_2 micro-nanometer composite with high specific surface area was synthesized by a facile solvothermal method. The high crystallinity of the product was obtained by heating it at 400°C for 2 h. The morphology of the as-prepared TiO_2 comprises microspheres and irregular aggregates with rather rough surfaces, which are composed of numerous nanocrystals. The primary particle size of this mesoporous TiO_2 is 10.2 nm. Its BET surface area is as high as 179 m^2 g^{-1} and the main pore sizes are in the range of 2–20 nm. The weak absorption on visible light, the sub-band-gap transition band in SPS, and the p-type semiconductor character (according to FISPS) of the mesoporous TiO_2 indicate there is surface impurity, which may derive from the raw material triethanolamine. The FT-IR spectrum shows there may be C–O or C–N groups on the TiO_2 surface, and XPS results confirm it is an N-doped TiO_2, where the N element is from triethanolamine. Under simulated sunlight irradiation, the photocatalytic activities of this mesoporous TiO_2 on both RhB and phenol aqueous solutions are higher than those of commercial TiO_2 (P25), which may be related with its high specific surface area, the light harvesting ability in visible region, mesoporous structure, and the existence of surface state. The as-prepared TiO_2 shows obvious photodegradation preference on RhB in the RhB-phenol mixture solution. Hence, RhB could not be

used as a sensitizer to increase the photocatalytic activity of phenol in visible light. Moreover, the sample TiO_2 can be easily reclaimed in 18 minutes by sedimentation from the suspension under gravity after photodegradation reactions. Thus, this TiO_2 catalyst is in favor of practical application in waste water treatment.

Acknowledgments

This work is supported by the National Natural Science Foundations of China (Grant no. 20871091), SRF for ROCS, SEM, the Open Project of Key Lab Advanced Energy Materials Chemistry (Nankai University) (KLAEMD-OP201201), and Tianjin Municipal Science & Technology Commission (07JCYBJC18600).

References

[1] W. G. Yang, F. R. Wan, Q. W. Chen, J. J. Li, and D. S. Xu, "Controlling synthesis of well-crystallized mesoporous TiO_2 microspheres with ultrahigh surface area for high-performance dye-sensitized solar cells," *Journal of Materials Chemistry*, vol. 20, no. 14, pp. 2870–2876, 2010.

[2] G. H. Wang, B. Cheng, J. Zhang, L. Xu, and T. T. Yin, "Facile synthesis and photocatalytic property of titania/carbon composite hollow microspheres with bimodal mesoporous shells," *International Journal of Photoenergy*, vol. 2012, Article ID 976389, 9 pages, 2012.

[3] J. S. Chen, Y. L. Tan, C. M. Li et al., "Constructing hierarchical spheres from large ultrathin anatase TiO_2 nanosheets with nearly 100% exposed (001) facets for fast reversible lithium storage," *Journal of the American Chemical Society*, vol. 132, no. 17, pp. 6124–6130, 2010.

[4] S. W. Liu, J. G. Yu, and M. Jaroniec, "Anatase TiO_2 with dominant high-energy 001 facets: synthesis, properties, and applications," *Chemistry of Materials*, vol. 23, no. 18, pp. 4085–4093, 2011.

[5] N. H. Lee, H. J. Oh, S. C. Jung, W. J. Lee, D. H. Kim, and S. J. Kim, "Photocatalytic properties of nanotubular-shaped TiO_2 powders with anatase phase obtained from titanate nanotube powder through various thermal treatments," *International Journal of Photoenergy*, vol. 2011, Article ID 327821, 7 pages, 2011.

[6] W. Zheng, X. Liu, Z. Yan, and L. Zhu, "Ionic liquid-assisted synthesis of large-scale TiO_2 nanoparticles with controllable phase by hydrolysis of $TiCl_4$," *ACS Nano*, vol. 3, no. 1, pp. 115–122, 2009.

[7] X. Zhang, J. H. Pan, A. J. Du, J. Ng, D. D. Sun, and J. O. Leckie, "Fabrication and photocatalytic activity of porous TiO_2 nanowire microspheres by surfactant-mediated spray drying process," *Materials Research Bulletin*, vol. 44, no. 5, pp. 1070–1076, 2009.

[8] J. A. Byrne, P. A. Fernandez-Ibañez, P. S. M. Dunlop, D. M. A. Alrousan, and J. W. J. Hamilton, "Photocatalytic enhancement for solar disinfection of water: a review," *International Journal of Photoenergy*, vol. 2011, Article ID 798051, 12 pages, 2011.

[9] M. H. Zhou, J. Zhang, B. Cheng, and H. G. Yu, "Enhancement of visible-light photocatalytic activity of mesoporous Au-TiO_2 nanocomposites by surface plasmon resonance," *International Journal of Photoenergy*, vol. 2012, Article ID 532843, 10 pages, 2012.

[10] S. Kumar, A. G. Fedorov, and J. L. Gole, "Photodegradation of ethylene using visible light responsive surfaces prepared from titania nanoparticle slurries," *Applied Catalysis B*, vol. 57, no. 2, pp. 93–107, 2005.

[11] F. Wei, H. Zeng, P. Cui, S. Peng, and T. Cheng, "Various TiO_2 microcrystals: controlled synthesis and enhanced photocatalytic activities," *Chemical Engineering Journal*, vol. 144, no. 1, pp. 119–123, 2008.

[12] L. Zhang, Y. Zhu, Y. He, W. Li, and H. Sun, "Preparation and performances of mesoporous TiO_2 film photocatalyst supported on stainless steel," *Applied Catalysis B*, vol. 40, no. 4, pp. 287–292, 2003.

[13] J. H. Xu, W. L. Dai, J. Li, Y. Cao, H. Li, and K. Fan, "Novel core-shell structured mesoporous titania microspheres: preparation, characterization and excellent photocatalytic activity in phenol abatement," *Journal of Photochemistry and Photobiology A*, vol. 195, no. 2-3, pp. 284–294, 2008.

[14] J. Luo and L. Gao, "Large-scale production of monodispersed titania microspheres by surfactant-guided self-assembly," *Journal of Alloys and Compounds*, vol. 487, no. 1-2, pp. 763–767, 2009.

[15] H. Zhang, Y. Han, X. Liu et al., "Anatase TiO_2 microspheres with exposed mirror-like plane 001 facets for high performance dye-sensitized solar cells (DSSCs)," *Chemical Communications*, vol. 46, no. 44, pp. 8395–8397, 2010.

[16] H. S. Hilal, L. Z. Majjad, N. Zaatar, and A. El-Hamouz, "Dye-effect in TiO_2 catalyzed contaminant photo-degradation: sensitization vs. charge-transfer formalism," *Solid State Sciences*, vol. 9, no. 1, pp. 9–15, 2007.

[17] Y. Cho and W. Choi, "Visible light-induced reactions of humic acids on TiO_2," *Journal of Photochemistry and Photobiology A*, vol. 148, no. 1–3, pp. 129–135, 2002.

[18] R. Comparelli, E. Fanizza, M. L. Curri et al., "Photocatalytic degradation of azo dyes by organic-capped anatase TiO_2 nanocrystals immobilized onto substrates," *Applied Catalysis B*, vol. 55, no. 2, pp. 81–91, 2005.

[19] E. M. Saggioro, A. S. Oliveira, T. Pavesi, C. G. Maia, L. F. V. Ferreira, and J. C. Moreira, "Use of titanium dioxide photocatalysis on the remediation of model textile wastewaters containing azo dyes," *Molecules*, vol. 16, no. 12, pp. 10370–10386, 2011.

[20] K. Sahel, N. Perol, F. Dappozze, M. Bouhent, Z. Derriche, and C. Guillard, "Photocatalytic degradation of a mixture of two anionic dyes: procion Red MX-5B and Remazol Black 5 (RB5)," *Journal of Photochemistry and Photobiology A*, vol. 212, no. 2-3, pp. 107–112, 2010.

[21] S. Liu, J. Yu, and M. Jaroniec, "Tunable photocatalytic selectivity of hollow TiO_2 microspheres composed of anatase polyhedra with exposed 001 facets," *Journal of the American Chemical Society*, vol. 132, no. 34, pp. 11914–11916, 2010.

[22] Q. Xiang, J. Yu, and M. Jaroniec, "Tunable photocatalytic selectivity of TiO_2 films consisted of flower-like microspheres with exposed 001 facets," *Chemical Communications*, vol. 47, no. 15, pp. 4532–4534, 2011.

[23] S. W. Liu, C. Liu, W. G. Wang, B. Cheng, and J. G. Yu, "Unique photocatalytic oxidation reactivity and selectivity of TiO_2-graphene nanocomposites," *Nanoscale*, vol. 4, pp. 3193–3200, 2012.

[24] L. Yanhong, W. Dejun, Z. Qidong, Y. Min, and Z. Qinglin, "A study of quantum confinement properties of photogenerated charges in ZnO nanoparticles by surface photovoltage spectroscopy," *Journal of Physical Chemistry B*, vol. 108, no. 10, pp. 3202–3206, 2004.

[25] L. Zhu, H. Miao, K. Liu, Y. Sun, M. Qiu, and X. Zhu, "Microwave and conventional hydrothermal synthesis of TiO_2 nanoparticles and their photocatalytic activities," *Advanced Materials Research*, vol. 391-392, pp. 988–992, 2012.

[26] Z. Li, M. Kawashita, and M. Doi, "Sol-gel synthesis and characterization of magnetic TiO_2 microspheres," *Journal of the Ceramic Society of Japan*, vol. 118, no. 1378, pp. 467–473, 2010.

[27] Wuhan University, *Instrument Analysis*, Higher Education Press, Beijing, China, 1st edition, 2001.

[28] X. Chen and C. Burda, "Photoelectron spectroscopic investigation of nitrogen-doped titania nanoparticles," *Journal of Physical Chemistry B*, vol. 108, no. 40, pp. 15446–15449, 2004.

[29] Y. Cong, J. Zhang, F. Chen, and M. Anpo, "Synthesis and characterization of nitrogen-doped TiO_2 nanophotocatalyst with high visible light activity," *Journal of Physical Chemistry C*, vol. 111, no. 19, pp. 6976–6982, 2007.

[30] F. Dong, H. Wang, and Z. Wu, "One-step "Green" synthetic approach for mesoporous C-doped titanium dioxide with efficient visible light photocatalytic activity," *Journal of Physical Chemistry C*, vol. 113, no. 38, pp. 16717–16723, 2009.

[31] T. C. Jagadale, S. P. Takale, R. S. Sonawane et al., "N-doped TiO_2 nanoparticle based visible light photocatalyst by modified peroxide sol-gel method," *Journal of Physical Chemistry C*, vol. 112, no. 37, pp. 14595–14602, 2008.

[32] C. Feng, Y. Wang, Z. Jin et al., "Photoactive centers responsible for visible-light photoactivity of N-doped TiO_2," *New Journal of Chemistry*, vol. 32, no. 6, pp. 1038–1047, 2008.

[33] Y. Wu, M. Xing, B. Tian, J. Zhang, and F. Chen, "Preparation of nitrogen and fluorine co-doped mesoporous TiO_2 microsphere and photodegradation of acid orange 7 under visible light," *Chemical Engineering Journal*, vol. 162, no. 2, pp. 710–717, 2010.

[34] Z. Lin, A. Orlov, R. M. Lambert, and M. C. Payne, "New insights into the origin of visible light photocatalytic activity of nitrogen-doped and oxygen-deficient anatase TiO_2," *Journal of Physical Chemistry B*, vol. 109, no. 44, pp. 20948–20952, 2005.

[35] I. N. Martyanov, S. Uma, S. Rodrigues, and K. J. Klabunde, "Structural defects cause TiO_2-based photocatalysts to be active in visible light," *Chemical Communications*, vol. 10, no. 21, pp. 2476–2477, 2004.

[36] L. Zhu, Y. Zheng, T. Hao, X. Shi, Y. Chen, and J. Ou-Yang, "Synthesis of hierarchical ZnO nanobelts via Zn(OH)F intermediate using ionic liquid-assistant microwave irradiation method," *Materials Letters*, vol. 63, no. 28, pp. 2405–2408, 2009.

[37] T. F. Xie, D. J. Wang, L. J. Zhu, T. J. Li, and Y. J. Xu, "Application of surface photovoltage technique in photocatalysis studies on modified TiO_2 photo-catalysts for photo-reduction of CO_2," *Materials Chemistry and Physics*, vol. 70, no. 1, pp. 103–106, 2001.

[38] X. Qian, D. Qin, Q. Song et al., "Surface photovoltage spectra and photoelectrochemical properties of semiconductor-sensitized nanostructured TiO_2 electrodes," *Thin Solid Films*, vol. 385, no. 1-2, pp. 152–161, 2001.

[39] L. Zhu, Y. Chen, Y. Sun et al., "Phase-manipulable synthesis of Cu-based nanomaterials using ionic liquid 1-butyl-3-methylimidazole tetrafluoroborate," *Crystal Research and Technology*, vol. 45, no. 4, pp. 398–404, 2010.

[40] Q. Zhao, D. Wang, L. Peng, Y. Lin, M. Yang, and T. Xie, "Surface photovoltage study of photogenerated charges in ZnO nanorods array grown on ITO," *Chemical Physics Letters*, vol. 434, no. 1–3, pp. 96–100, 2007.

[41] P. F. Lee, X. Zhang, D. D. Sun, J. Du, and J. O. Leckie, "Synthesis of bimodal porous structured TiO_2 microsphere with high photocatalytic activity for water treatment," *Colloids and Surfaces A*, vol. 324, no. 1–3, pp. 202–207, 2008.

[42] A. J. Maira, K. L. Yeung, C. Y. Lee, P. L. Yue, and C. K. Chan, "Size effects in gas-phase photo-oxidation of trichloroethylene using nanometer-sized TiO_2 catalysts," *Journal of Catalysis*, vol. 192, no. 1, pp. 185–196, 2000.

[43] K. L. Lv, B. Cheng, J. G. Yu, and G. Liu, "Fluorine ions-mediated morphology control of anatase TiO_2 with enhanced photocatalytic activity," *Physical Chemistry Chemical Physics*, vol. 14, no. 16, pp. 5349–5362, 2012.

[44] S. W. Liu, J. G. Yu, B. Cheng, and M. Jaroniec, "Fluorinated semiconductor photocatalysts: tunable synthesis and unique properties," *Advances in Colloid and Interface Science*, vol. 173, pp. 35–53, 2012.

[45] Q. Wang, C. Chen, D. Zhao, M. Wanhong, and J. Zhao, "Change of adsorption modes of dyes on fluorinated TiO_2 and its effect on photocatalytic degradation of dyes under visible irradiation," *Langmuir*, vol. 24, no. 14, pp. 7338–7345, 2008.